Dyes and Pigments 94 (2012) 355–362

Contents lists available at SciVerse ScienceDirect

Dyes and Pigments

journal homepage: www.elsevier.com/locate/dyepig

Au–Ag nanoparticles as red pigment in ceramic inks for digital decoration

M. Blosi [a,*], S. Albonetti [b,c], F. Gatti [b], G. Baldi [d], M. Dondi [a]

[a] Institute of Science and Technology for Ceramics (ISTEC-CNR), Via Granarolo 64, 48018 Faenza, Italy
[b] Department of Industrial Chemistry and Materials, University of Bologna, Viale Risorgimento 4, 40136 Bologna, Italy
[c] INSTM, Research Unit of Bologna, Viale Risorgimento 4, 40136 Bologna, Italy
[d] CERICOL, Colorobbia Research Centre, Via Pietramarina 123, 50053 Sovigliana Vinci, Italy

ARTICLE INFO

Article history:
Received 29 August 2011
Received in revised form
20 December 2011
Accepted 11 January 2012
Available online 24 January 2012

Keywords:
Ag
Au
Ceramic pigment
Ink
Nanoparticles

ABSTRACT

Novel pigments, consisting of Au–Ag mixed nanoparticles, were developed for digital decoration by ink-jet printing of ceramic wares. Special attention was paid to set up a microwave assisted synthesis route, with a low environmental impact, easily transferable to large-scale production. Several suspensions, based on Au, Ag and Au–Ag mixed nanoparticles were prepared, trying to get a core-shell assemblage, and the synthesis parameters like metal concentration, Ag/Au ratio, time, temperature and chelating agent amount were optimized. The suspensions are stable over many months and a total reaction yield, assessed by ICP-AES analysis, was achieved. Particle size, shape, composition and optical properties were measured by DLS, TEM-EDS, XRD and UV–VIS spectroscopy. The so-prepared inks were applied on ceramic tiles simulating the ceramic process and the colour performance, assessed by colourimetry, were expressed in the CIELab parameters.

1. Introduction

Metal nanoparticles represent an efficient way to bestow yellow to red coloration on glass and transparent glazes [1–3]. Colour is developed through the mechanism of surface plasmon resonance (SPR) – although it depends also on particle size, particles inter-distance, alternating dielectric and metal particles-bearing layers [1] – which is due to charge-density oscillations confined to metal nanoparticles [4,5]. The excitation of surface plasmons by an electric field at an incident wavelength, where resonance occurs, results in strong light scattering, appearance of intense SPR absorption bands, and enhancement of the local electromagnetic field. The frequency (i.e. absorption maxima and therefore colour) and intensity of SPR bands are characteristic of each metal and highly sensitive to particle size and shape [4–7].

As a matter of fact, nanodispersions of Au, Ag and Cu were used to colour glass and lustre glassy coatings since Roman times [8], and particularly during the Middle Age [9–11] and the Renaissance [12–14]. This property of noble metals has been recently exploited by the ceramic industry through digital decoration techniques, primarily ink-jet printing, which make use of gold nanopigments [15,16]. Current technology of metal inks for ceramics encompasses various approaches: (i) application of gold precursors then in-situ nucleation and growth of Au crystals inside the glassy matrix [17,18]; (ii) synthesis of gold nanoparticles by polyol method and application as ceramic pigment [15,19]. These Au nanopigments proved to be particularly stable in a wide range of firing temperatures (up to 1200 °C) and chemical environments (different glazes, glassy coatings and porcelain stoneware bodies) [16].

However, a strong limitation to gold inks stems from their high cost, even if efficient colouring performance is achieved with very low Au concentrations [15,16]. From this standpoint, industry can take advantage by using silver instead of gold, as Ag is less expensive than Au by a factor of ~50. In addition, inks containing both silver and gold are expected to exhibit different optical properties, as the energy of SPR bands changes with the Au/Ag ratio [1–4]. Moreover, these features may have a beneficial effect on the technological behaviour of inks, e.g. improving their colouring performance.

In this paper, we present a simple microwave-assisted route for producing gold, silver and Au–Ag structures in the form of stable nanosuspensions [20] assessing their suitability as ceramic colorant. Control of particle size and colloidal stability was pursued through accurate reaction optimization combined with microwave heating, in order to get a significant process intensification, on a large scale production too. In fact, both low environmental impact and long time stability of suspensions can turn into a breakthrough for industrial scale up.

* Corresponding author. Tel.: +39 0546699718.
E-mail address: magda.blosi@istec.cnr.it (M. Blosi).

0143-7208/$ – see front matter © 2012 Elsevier Ltd. All rights reserved.
doi:10.1016/j.dyepig.2012.01.006

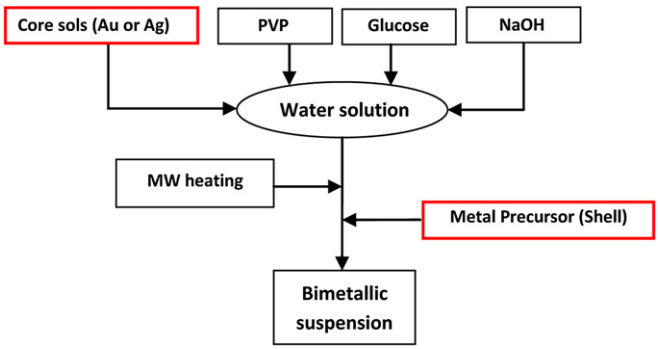

Fig. 1. Synthesis flow chart of bimetallic nanoparticles.

Table 1
Composition of prepared bimetallic nanoparticles.

Sample	%Au (mol/mol)	%Ag (mol/mol)	Ag/Au (mol/mol)	Metals Conc. (mol/L)
Au	100	0	–	0.011
Au-80	100	0	–	0.011
$(Au)_{67}Ag_{33}$	67	33	0.5	0.015
$(Au)_{40}Ag_{60}$	40	60	1.5	0.008
$(Au)_{18}Ag_{82}$	18	82	4.5	0.006
Ag	0	100	–	0.05
$(Ag)_{33}Au_{67}$	67	33	0.5	0.015
$(Ag)_{60}Au_{40}$	40	60	1.5	0.008
$(Ag)_{82}Au_{18}$	18	82	4.5	0.006

2. Experimental

2.1. Synthesis of bimetallic nanoparticles

Au/Ag nanoparticles were prepared by a two-step method, with the purpose to get core-shell nanostructures, characterized by synthesis of the shell on the preformed core, which acts as a seed of nucleation (Fig. 1). Either Au or Ag sols were used as core: labels indicate metal at the core (in brackets) while subscripts are referred to the molar composition (Table 1). Two series, differing for the metal core (Au-core, Ag-core) were synthesized and for each series three silver/gold molar ratios were prepared: 0.5, 1.5, 4.5.

Table 2
Chemical composition and physical properties of the transparent (F5) and the matt (S2) glazes.

Component/Property	Unit	F5	S2
SiO_2	% wt.	59.0	51.1
B_2O_3	% wt.	2.0	1.2
Al_2O_3	% wt.	9.0	22.6
MgO	% wt.	2.0	1.4
CaO	% wt.	12.0	13.5
ZnO	% wt.	11.0	5.1
BaO	% wt.	<0.5	1.4
Na_2O	% wt.	1.0	2.6
K_2O	% wt.	4.0	0.6
Maturing temperature (softening) T_1	°C	1010	1150
Temperature of half sphere T_2	°C	1170	1200
Temperature of melting T_3	°C	1220	1235
Viscosity at T_1	kPa s	4.28	4.97
Surface tension at T_1	mN m^{-1}	363	394
Refractive index	1	1.546	1.547
Coeff. thermal expansion $\alpha_{20-400°C}$	MK^{-1}	6.21	5.54
Theoretical density	g cm^{-3}	2.719	2.775

Table 3
Physical characteristics of the synthesized samples: mean particle diameter by Dynamic Light Scattering (∅DLS) and Transmission Electron Microscopy (∅TEM); Polydispersion Index (PDI); Reaction yield (% of crystalline metal formed).

Sample	∅DLS (nm)	PDI (1)	∅TEM (nm)	Stand. Dev (nm)	Reaction yield (%wt)
Au	16	0.3	7	3	99.8
Au-80	24	0.8	–	–	99.6
$(Au)_{67}Ag_{33}$	29	0.3	6	2	99.8
$(Au)_{40}Ag_{60}$	32	0.2	9	4	99.8
$(Au)_{18}Ag_{82}$	36	0.2	12	4	99.7
Ag	65	0.2	18	3	99.8
$(Ag)_{33}Au_{67}$	62	0.2	–	–	99.9
$(Ag)_{60}Au_{40}$	66	0.3	–	–	99.8
$(Ag)_{82}Au_{18}$	67	0.3	–	–	99.7

Au-core and Ag-core sols, exploited as seeds, were obtained separately throughout the reduction of $HAuCl_4$ or $AgNO_3$ by D(+) glucose in alkaline water. PVP-coated metal seeds were synthesized by microwave heating, following a patented procedure [20]. The typical procedure used to synthesize gold or silver seeds

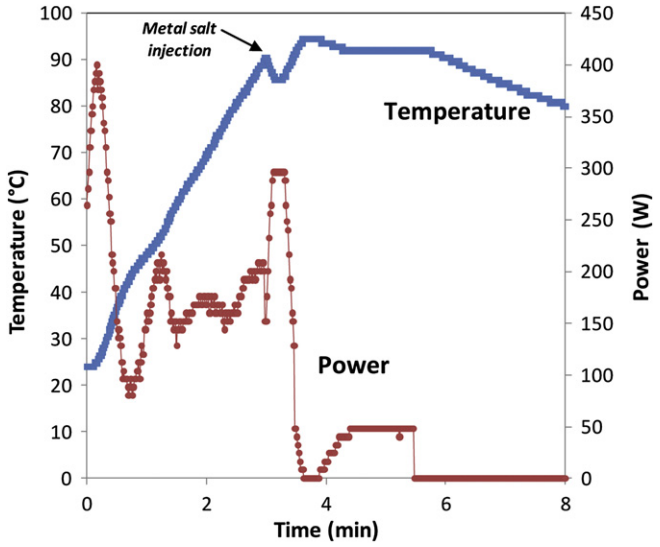

Fig. 2. Temperature and output power profile during microwave heating at 90 °C for 5 min.

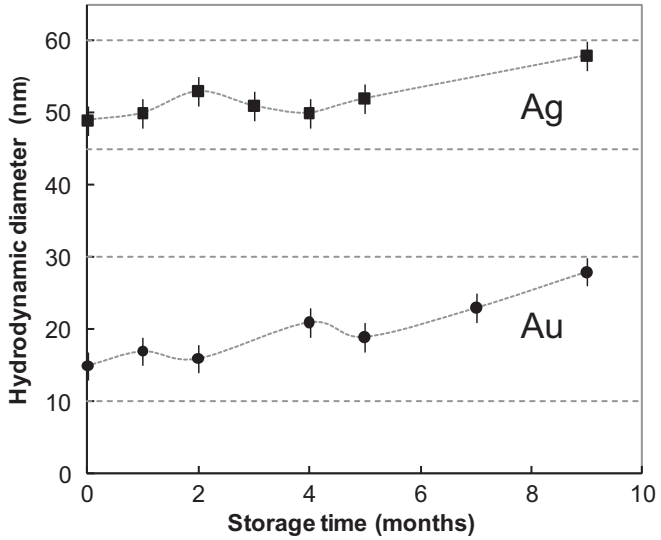

Fig. 3. Hydrodynamic diameter measured by dynamic light scattering (DLS) for Au and Ag suspensions, during the storage time.

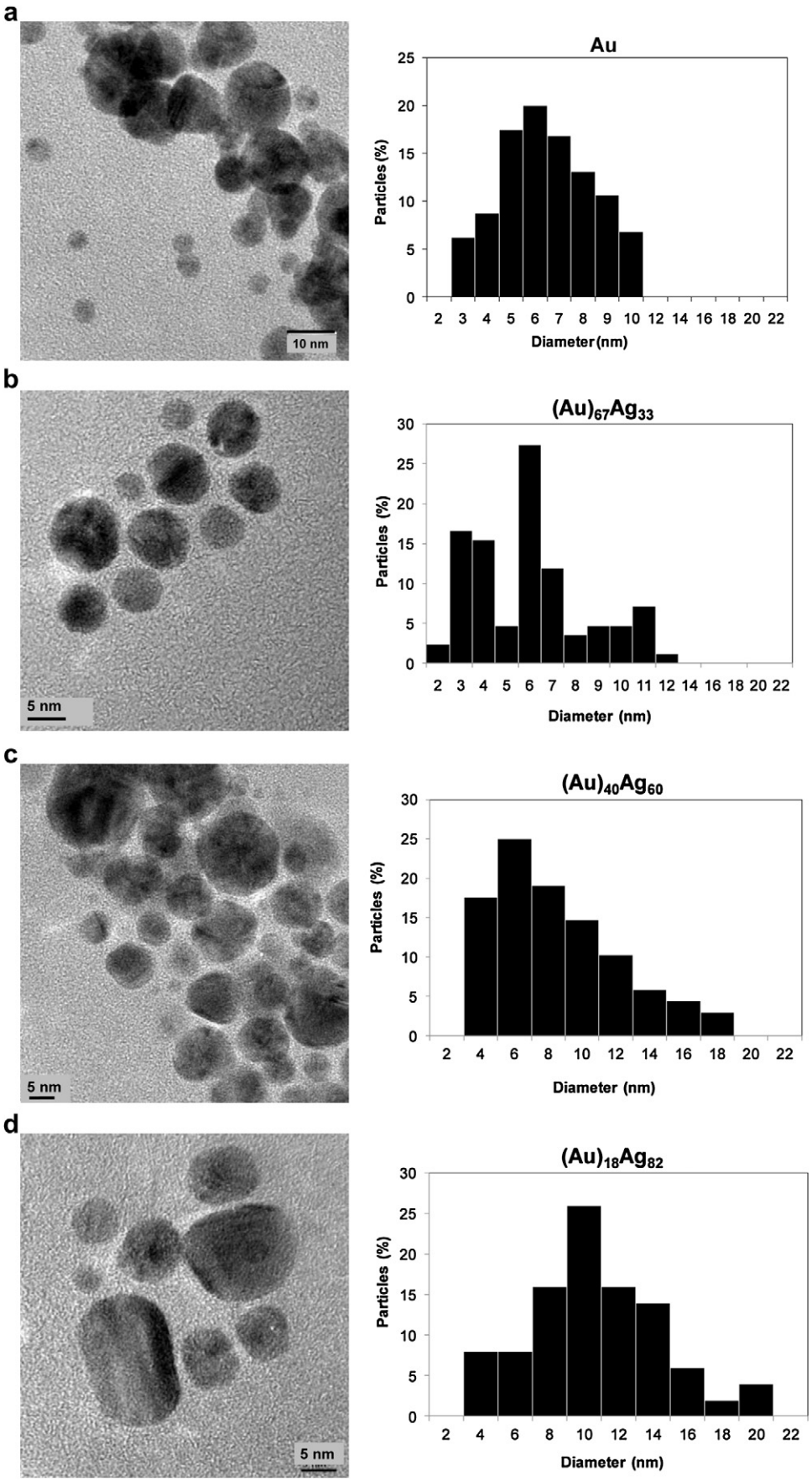

Fig. 4. TEM images of gold nanoparticles (a) and of Au core samples: $(Au)_{67}Ag_{33}$; (b); $(Au)_{40}Ag_{60}$ (c); $(Au)_{18}Ag_{82}$ (d).

requires a water solution containing the chelating agent (polyvinylpirrolidone, PVP, Mw 29,000), the reducing agent [D(+) glucose] and the needed amount of NaOH in order to maintain a pH of 6 (for Ag) and of 9 (for Au). Such a solution was heated till the synthesis temperature: 70 °C (for Ag), and 90 °C (for Au). Then, a second solution, containing the metal salt, was poured into the hot solution, keeping the synthesis temperature for 5 min and obtaining a total metal concentration ranging between 0.008 and 0.011 M depending on the composition and the Ag/Au molar ratio. By this way, the metal salts were reduced to metallic nanoparticles and a red or a yellow suspension was obtained for gold or silver nanoparticles, respectively. For each material, the control on particle size was exerted by careful optimization of the solution pH (kept between 6 and 9) and some fundamental molar ratios: the chelating agent to metal ratio (ranging from 2.5 to 5.5) and the glucose to metal ratio (comprised between 3 and 1). Shell metals were synthesized exploiting the previously prepared seeds as solvent and by using the same parameters optimized for seeds.

A microwave apparatus (MicroSYNTH plus, Milestone, Italy) – whose reaction chamber is provided with magnetic stirring, reflux system, optical fibre temperature controller and a glass container – was used (microwave power generated by 2 × 800 W magnetrons with frequency 2.45 GHz). In order to match the scheduled heating ramp, the power is continuously supplied and automatically modulated by a software to follow the temperature profile; for each ramp only the maximum deliverable power can be imposed. A typical temperature and output power profile, for a reaction at 90 °C, is shown in Fig. 2.

2.2. Characterization of suspensions and nanoparticles

Metal nanosuspensions were characterized for reaction yield, optical properties, phase composition, particle size and microstructure.

Unreacted metal cations were analyzed by ICP-AES in order to determine the reaction yield. Samples were prepared as follow: 50 ml of synthesized colloid was poured into a semi-permeable osmotic membrane (Visking tube) which was immersed in a de-ionized water bath. Osmotic pressure caused the exchange of unreacted cations into the external liquid. After 3 h, the equilibrium was attained and the external liquid underwent ICP (Liberty 200, Varian, Australia) quantitative analyses (Au line 267.595 Å, Ag line 328.068 Å, plasma power 1.20 kW, plasma flow 15 L min^{-1}, sample pump rate 15 rpm).

UV–VIS extinction spectra were measured with a Lambda 35 spectrophotometer (Perkin Elmer, UK), using a quartz cuvette as sample-holder. Samples were prepared by diluting the as prepared colloidal suspension with water in order to get into the cuvette the same metal concentration for every sample.

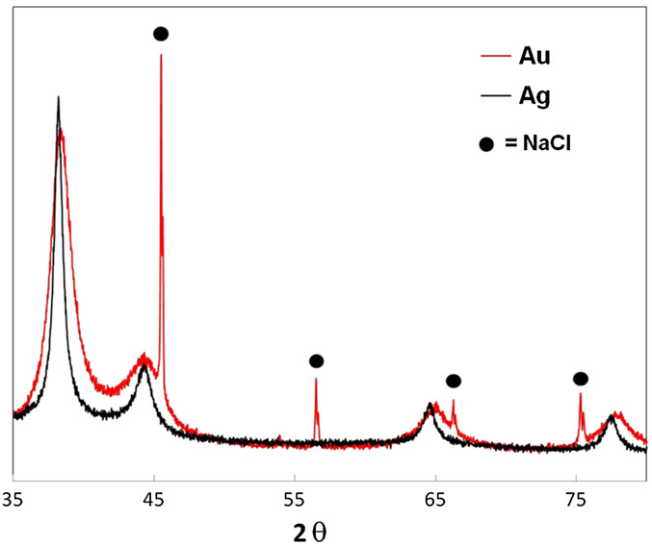

Fig. 5. XRD spectra of gold and silver nanoparticles (the narrow peaks correspond to NaCl formed as byproduct during the synthesis of gold).

Diffraction patterns were collected on the synthesized samples dripped on a glass slide and dried at 100 °C for 5 min (D8 Advance, Bruker, Germany) operating with *a LynxEye* detector (20–80° 2θ range, 0.02 s^{-1}, 0.5 s time-per-step).

Particle size distribution, based on hydrodynamic diameter, was evaluated by dynamic light scattering (DLS, Nano S, Malvern, UK) equipped with He–Ne laser (wavelength 633 nm) taking care to dilute the sample with water and pour it in a polystyrene cuvette before measurement. Hydrodynamic diameter includes both the coordination sphere and the species adsorbed on particle surface, such as stabilizers, surfactants and so forth. DLS analysis provides also a polydispersion index parameter (PDI), ranging from 0 to 1, quantifying of the colloidal dispersion degree; samples can be considered monodispersed for PDI values lower than 0.2.

The investigation of the particle size distribution was performed using a Transmission Electron Microscope (TEM, Tecnai F20, FEI, The Netherlands) combining electron imaging and STEM mode with EDX microanalysis. Nanoparticles were dispersed on a standard copper grid for TEM investigation by simple drop-casting of the prepared solutions. Samples were left to dry (air atmosphere) then placed on a hot-plate at 100 °C for 5 min to ensure the complete evaporation of water before TEM analysis.

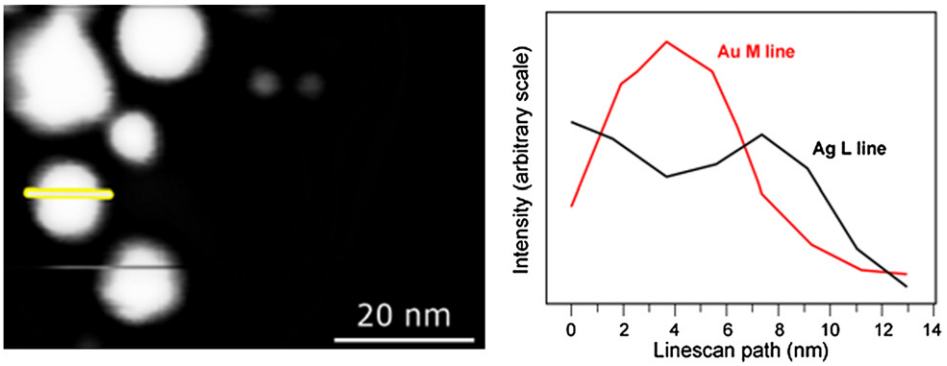

Fig. 6. STEM line scanning across a nanoparticle of sample $(Au)_{18}Ag_{82}$ and corresponding EDX profile.

2.3. Application as ceramic inks

The industrial tile decoration process (e.g. by ink-jet printing) was simulated at the laboratory scale: ceramic tiles were glazed, then decorated by using an aerospray gun and fired in an electric roller kiln (maximum temperature: 1150 °C, 5 min soaking, 50 min cold-to-cold). Two different coatings (F5 transparent and S2 opaque) were tested (Table 2). In order to get the same metal concentration, the suspensions were diluted and applied taking care that each tile did receive the same amount of pigment (0.2 g m^{-2}).

Decorated tiles were characterized by colourimetry and X-ray diffraction (XRD). The colour was measured by diffuse reflectance spectroscopy (Miniscan MSXP4000, Hunter Lab, USA) in the 400–700 nm range (illuminant D65, observer 10°) taking a white glazed tile as reference (CIE $x = 31.5$, $y = 33.3$). Colour is expressed in the CIELab parameters: brightness (L^* 100 = white, 0 = black) and chroma (a^* = red +, green −; b^* = yellow +, blue −). The occurrence of metal nanoparticles after ceramic processing was verified by XRD on the glaze surface (Geigerflex, Rigaku, 38–39° 2θ range, 0.02 s^{-1}, 10 s time-per-step). The size of coherent diffraction domains, considered to be a good estimation of crystallite dimension, was calculated by Scherrer's equation [21] using FWHM (Full Width at Half Maximum) of the [111] peak; instrumental broadening was corrected by measuring the LaB_6 reference material (NIST SRM660a).

3. Results and discussion

3.1. Synthesis and stability of nanosuspensions

In all samples the reaction yield is over 99%, indicating that the optimized synthesis succeeded in the complete reduction of precursors (Table 3). Reaction yield represents a key point for large scale production in order to both optimize the process and know the actual solid content of suspensions [22].

Suspensions with excellent stability, up to several months of storage, were obtained for both seeds and mixed sols, implying that no significant particles aggregation occurred. Since it is expected that the time stability of mixed suspensions is strictly dependent on the colloidal stability of core sol, which acts as support for the subsequent shell nucleation, the hydrodynamic particle diameter was measured during the storage (Fig. 3). For both metals, the hydrodynamic diameter remained practically unchanged for the first five months, indicating that no aggregation occurred; moreover, no precipitation was observed up to 12 months. As consequence, also bimetallic nanosuspensions show a long time stability: in fact, no precipitation occurred till 7 months after synthesis.

The hydrodynamic diameter of Au nanoparticles is smaller than that of Ag ones. Bimetallic samples containing a growing silver amount exhibit a progressive increase of particle size. For all samples, the polydispersion index indicates a narrow distribution. Overall, the diameter of the particles used as seed governs the final

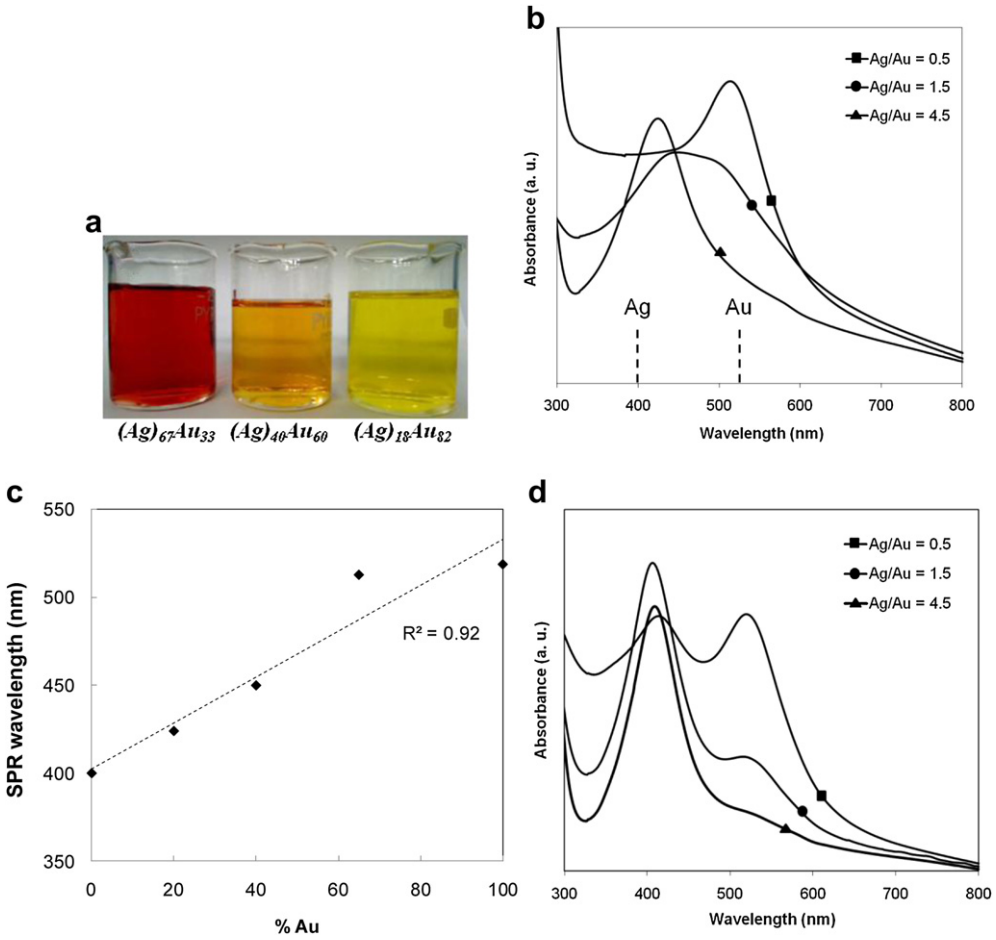

Fig. 7. a) Color shift observed at different metal composition in Ag-core series; b) UV-VIS absorbance spectra of Ag-core series; c) linear correlation between surface plasmon resonance wavelength and particle composition; d) UV-VIS absorbance spectra of Au and Ag suspensions physically mixed by following the same molar ratios of the synthesized samples.

size: Au-core bimetallic particles are always finer than Ag-core ones (Table 3).

3.2. Nanoparticle characterization

HRTEM observations prove that the actual particle size of noble metals is finer than the hydrodynamic diameter (Table 3) which comprises the coordination sphere [23]. For gold and Au-core particles, HRTEM shows a mean diameter below 12 nm (Fig. 4). As evidenced by both HRTEM and DLS, samples containing a higher concentration of shell element exhibit a slight increase in the mixed particle diameter, suggesting that reduction/deposition, rather than other phenomena, dominates the coating process.

XRD patterns show the characteristic peaks of gold and silver (Fig. 5) as well as the peak broadening typical of nano-sized crystallites, which mean size was estimated to be ~5 nm for gold and ~10 nm for silver, so confirming the coarser size of Ag nanoparticles (reasonably matching TEM data: 7 and 18 nm for Au and Ag particles, respectively). The Au pattern shows sharp peaks of NaCl, a byproduct of the reaction, which can be easily removed by a washing-filtration process. Since Ag and Au have the same crystal structure (space group Fm-3m) and unit cell parameter very close each other ($a = 4.086$ Å for silver, $a = 4.072$ Å for gold) [24] it was not possible to discriminate the single contribution of each metal in bimetallic patterns.

EDX-STEM line scanning, carried out to map the chemical composition across the nanoparticles, supports the presence of an Au_{core}/Ag_{shell} nanostructure, although the distribution of gold appears to be rather heterogeneous. In the sample $(Au)_{18}Ag_{82}$, for instance, the Au concentration is maximum at the core, while the Ag concentration is prevailing at the shell (Fig. 6).

As known from the literature, the SPR of noble metal nanoparticles induces a strong absorption in the visible region that is strictly linked to particles size and shape [24–28]. Nevertheless, the SPR band is suppressed for coarser particles, because they turn more similar to the bulk state [29–31]. Since each metal has its typical absorption wavelength due to SPR [24], the composition does strongly affect optical properties: for bimetallic particles the suspensions acquire different colours by changing the Au/Ag ratio (Fig. 7a). For this reason, while the Au nanoparticles solution has a characteristic SPR peak at 520 nm, bimetallic samples with increasing silver content exhibit a gradual blue shift towards the value of 400 nm, i.e. the characteristic SPR energy of silver (Fig. 7b). Since for a physical mixing of two metals, as shown in Fig. 7d, two distinct bands would be observed [5], the SPR shift, shown by the Ag_{core} series in Fig. 7b, confirms the formation of bimetallic nanoparticles in which gold and silver interact with each other, causing a clear change of plasmonic band energy.

3.3. Colouring performance as ceramic inks

The colour of pigment-bearing coatings (Table 4) depends on many factors, including gold concentration, Au/Ag ratio, nanoparticle structure (Au_{core} or Au_{shell}), particle shape, dielectric constant and vitreous-to-crystalline-phases ratio of the matrix. Anyway, colour is a nearly pure red (a^*) with a limited yellow component (b^*); saturation varies firstly in function of the kind of coating (L^* is lower in the transparent glaze than in the opacified one) and secondly of the amount of gold.

The red component is directly correlated with gold concentration, even if a^* values generally do not furtherly grow when Au content increases approximately over 0.13% Au. Bimetallic nanopigments behave similarly to Au nanoparticles (Fig. 8) in both transparent and opaque coatings. Their colouring performance, in fact, is nearly the same of gold nanoparticles given the same Au concentration.

$Au_{shell}Ag_{core}$ nanopigments are characterized by a better colouring performance with respect to $Au_{core}Ag_{shell}$ ones. In particular, $Au_{shell}Ag_{core}$ with 0.04% Au and 1.5 Au/Ag ratio exhibits the best behaviour for both transparent and opaque glazes, as its colouring performance is practically the same of nanopigments with gold concentration over 0.1%.

Silver seems not to affect significantly the colour quality and, despite the deep yellow shade of Ag nanoparticles suspensions, little contribution is given to the pigment-bearing coatings in terms of yellow component (b^*).

Table 4
Colouring performance of Au and AuAg nanopigments into opaque and transparent coatings (CIE L*a*b*).

Sample	Au (wt%)	Opaque glaze			Transparent glaze			Crystallite size (nm)[a]
		L^*	a^*	b^*	L^*	a^*	b^*	
Au	0.04	82.9	4.1	0.6	64.9	22.7	−1.1	58
Au	0.13	77.0	9.3	0.4	49.7	29.2	0.1	94
Au	0.20	75.5	8.4	−0.1	48.8	30.4	0.2	99
$(Ag)_{33}Au_{67}$	0.19	82.3	6.0	1.4	61.1	25.5	−0.4	82
$(Ag)_{33}Au_{67}$	0.20	74.1	11.3	1.5	49.3	29.4	2.4	86
$(Ag)_{60}Au_{40}$	0.08	78.9	8.8	0.7	59.4	27.3	−0.4	56
$(Ag)_{60}Au_{40}$	0.07	82.6	6.5	0.9	64.0	23.8	−0.8	74
$(Ag)_{82}Au_{18}$	0.03	88.7	2.7	2.3	71.5	28.4	2.4	61
$(Au)_{67}Ag_{33}$	0.19	84.9	5.0	1.4	62.5	24.7	−0.9	56
$(Au)_{67}Ag_{33}$	0.20	81.3	6.1	0.6	50.9	29.4	−0.2	83
$(Au)_{40}Ag_{60}$	0.07	88.1	2.4	1.3	68.7	20.9	−1.4	82
$(Au)_{40}Ag_{60}$	0.08	86.4	2.5	0.9	64.9	23.1	−1.5	72

[a] crystallite size is referred to the transparent glaze.

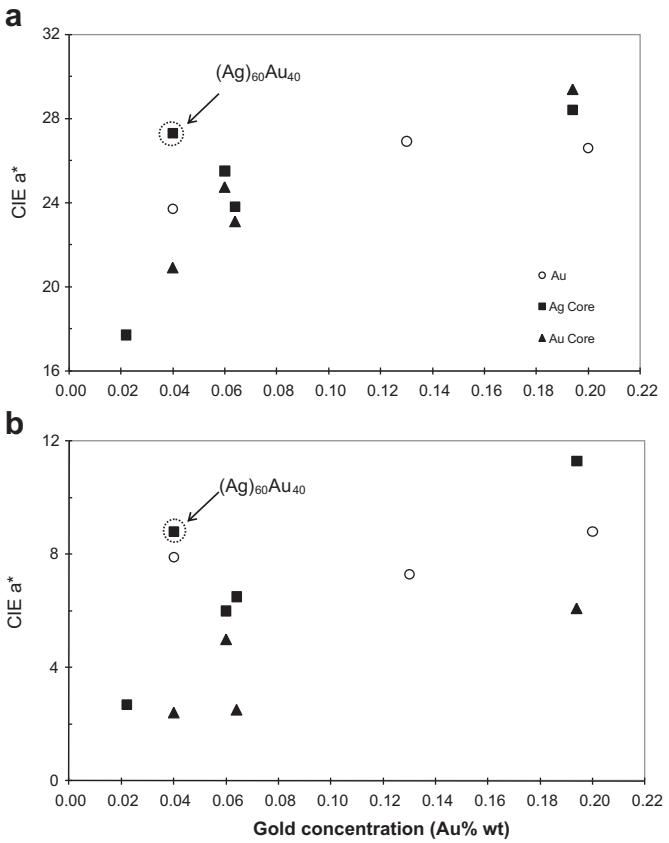

Fig. 8. CIEa^* values for gold and bimetallic nanoparticles at different gold content for vitreous (a) and matt (b) coating.

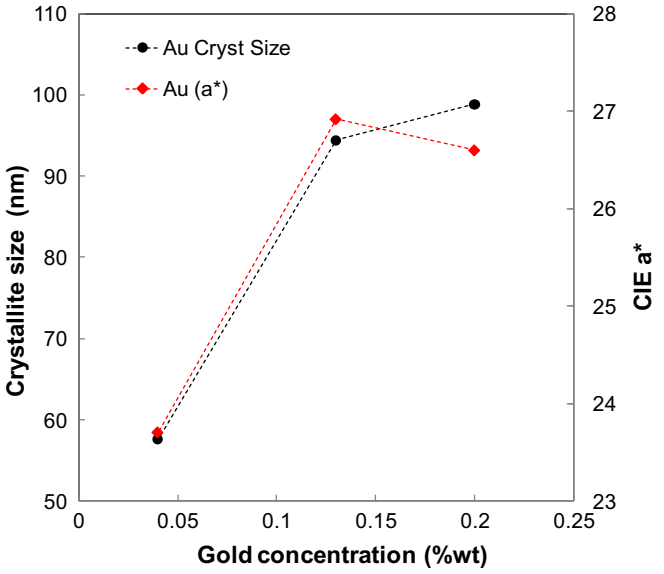

Fig. 9. Gold crystallite size and CIEa^* values for different metal concentrations.

The crystallite size of nanopigments presents, after firing, an increment with metal concentration, with a marked trend for gold (Table 4). Probably, the crystallite growth at higher concentration is due to a more frequent occurrence of particle coalescence. Since colour performance of nanometric pigment is strictly related to their particle size, variations of crystallite size induce a colour change. Unexpectedly, a^* values for gold samples do not increase proportionally with Au concentration, attaining a maximum value for intermediate metal content (Fig. 9). This circumstance is explained by the fact that particles with higher metal concentration grow faster, causing a detrimental effect on the red component (a^*) because SPR bands have a reduced intensity in coarse particles. As a result, gold concentration and red performance have to be set in order to achieve the optimized red colour, avoiding a useless increasing of metal concentration. Basically, for bimetallic particles the trend of crystallite growth with metal concentration is respected, besides the relationships between crystallite size and colour performance is not as conspicuous as in gold. This occurs because of the simultaneous presence of silver and gold, at different ratios, with different core-shell assemblages.

4. Conclusions

Stable bimetallic nanosuspensions (Au–Ag) were developed by using a simple and eco-friendly method. Its low environmental impact, together with the long time stability of suspensions, represent a great advantage, making this process suitable for large scale production. As a matter of fact, by dealing with suspensions it is possible on the one side to avoid nanopowders in the working ambient and to the other side to set up a continuous flow process. Microwave heating was developed for large scale production; pilot plant tests showed satisfactory results, enabling the desired process intensification to improve its efficiency and efficacy.

The synthesis of bimetallic nanostructures provided a rather wide range of particle size and optical properties. It is a versatile route which allows to easily change particles size and composition only by tuning the process parameters.

Nanopigments so synthesized are suitable for application as ceramic inks for digital decoration. A set of red colours with different shades can be obtained in both transparent and opacified glazes. Particle growth, caused by firing, is faster for higher metal concentration; this phenomenon is clearly observed in gold samples, in which a particle coarsening induced a deterioration of colour performance.

In particular, the nanopigment $Au_{shell}Ag_{core}$ with a 1.5 Au/Ag ratio and an Au concentration of 0.04% has a colouring performance very similar to gold inks with a concentration over 0.1%. This implies a substantial cost advantage by reducing the gold content in favour of silver. Further analysis on this material is now ongoing, in order to better understand the role of silver when used as core.

References

[1] Colomban P. The use of metal nanoparticles to produce yellow, red and iridescent colour, from bronze age to present times in lustre pottery and glass: solid state chemistry, spectroscopy and nanostructure. J Nano Res 2009;109:132–8.
[2] Lafait J, Berthier S, Andraud C, Reillon V, Boulenguez J. Physical colors in cultural heritage: surface plasmons in glass. Compt Rend Phys 2009;10:649–59.
[3] Vosburgh J, Doremus RH. Optical absorption spectra of gold nano-clusters in potassium borosilicate glass. J Non-Cryst Solids 2004;349:309–14.
[4] Moores A, Gotmanns F. The plasmon band in noble metal nanoparticles: an introduction to theory and applications. New J Chem 2006;30:1121 [32].
[5] Wilcoxon JP, Abrams BL. Synthesis, structure and properties of metal nano-clusters. Chem Soc Rev 2006;35:1162–94.
[6] Pradell T, Molera J, Bayés C, Roura P. Luster decoration of ceramics: mechanisms of metallic luster formation. Appl Phys A 2006;203:08–83.
[7] Rao CNR, Kulkarni GU, Thomas PJ, Edwards PP. Metal nanoparticles and their assemblies. Chem Soc Rev 2000;29:27–35.
[8] Reboulleau MEF, Magnier MD. Nouveau Manuel complet de la peinture sur verre, sur porcelaine et sur email, des emaillages industriels et de la fabrication des emaux et des Couleurs vitrifiables. Paris: Encyclopedie-Roret; 1913.
[9] Molera J, Bayés C, Roura P, Crespo D, Pradell T. Key parameters in the production of medieval luster colors and shines. J Am Ceram Soc 2007;2245:54–90.
[10] Pradell T, Molera J, Pantos E, Smith AD, Martin CM, Labrador A. Temperature resolved reproduction of medieval luster. Appl Phys A 2008;81:88–90.
[11] Padovani S, Puzzovio D, Sada C, Mazzoldi P, Borgia I, Sgamellotti A, et al. XAFS study of copper and silver nanoparticles in glazes of medieval middle-east lustreware (10th–13th century). Appl Phys A 2006;83:521–8.
[12] Darque-Ceretti E, Helary D, Bouquillon A, Aucouturier M. Gold like lustre: nanometric surface treatment for decoration of glazed ceramics in ancient Islam, Moresque Spain and Renaissance Italy. Surf Eng 2005;21:352–8.
[13] Padovani S, Borgia I, Brunetti B, Sgamellotti A, Giulivi A, D'Acapito F, et al. Silver and copper nanoclusters in the lustre decoration of Italian Renaissance pottery: an EXAFS study. Appl Phys A 2004;229:33–79.
[14] Padeletti G, Fermo P. Production of gold and ruby-red lustres in Gubbio (Umbria, Italy) during the Renaissance period. Appl Phys A 2004;241:45–79.
[15] Gardini D, Dondi M, Costa AL, Matteucci F, Blosi M, Galassi C, et al. Nano-sized ceramic inks for drop-on-demand ink-jet printing in quadrichromy. J Nanosci Nanotech 2008;8:1979–88.
[16] Cavalcante PM, Dondi M, Guarini G, Raimondo M, Baldi G. Colour performance of ceramic nano-pigments. Dyes Pigm 2009;226:32–80.
[17] Heathcote R, Howell JAS, Jennings N, Cartlidge D, Cobden L, Coles S, et al. Gold(I)-isocyanide and gold(I)-carbene complexes as substrates for the laser decoration of gold onto ceramic surfaces. Dalton Trans 2007;13:1309–15.
[18] Paganelli M. Glazing and decoration of ceramic tiles. Modena: Sala, Italian Ceramic Society; 2000.
[19] Baldi G, Bitossi M, Barzanti A. Patent WO 03/076521 A1; 2003.
[20] Blosi M, Albonetti S, Dondi M, Baldi G, Barzanti A. Process for preparing stable suspensions of metal nanoparticles and the stable colloidal suspensions obtained thereby. WO 2010/100107 PCT/EP2010/052534.
[21] Patterson AL. The Scherrer formula for X-ray particle size determination. Phys Rev 1939;56:978–82.
[22] Blosi M, Albonetti S, Dondi M, Martelli C. Microwave-assisted polyol synthesis of Cu nanoparticles. J Nanopart Res 2011;13:127–38.
[23] Suh IK, Ohta H, Waseda Y. High-temperature expansion of six metallic elements measured by dilatation method and X-ray diffraction. J Mater Sci 1988;23:757–60.
[24] Kreibig U, Genzel L. Optical absorption of small metallic particles. Surf Sci 1985;156:678–700.
[25] Lisiecki I, Billoudet F, Pileni MP. Control of the shape and the size of copper metallic particles. J Phys Chem 1996;4160:66–100.
[26] Sönnichsen C, Franzl T, Wilk T, Von Plessen G, Feldmann J. Drastic reduction of plasmon damping in gold nanorods. Phys Rev Lett 2002;88:77402 [1/4].
[27] Berciaud S, Cognet L, Tamarat P, Berciaud BL. Observation of intrinsic size effects in the optical response of individual gold nanoparticles. Nano Lett 2005;515:18–25.
[28] Gaikwad AV, Verschuren P, Eiser E, Rothenbe G. A simple method for measuring the size of metal nanoclusters in solution. J Phys Chem B 2006;17437:43–110.

[29] Yeh MS, Yang YS, Lee YP, Lee HF, Yeh YH, Yeh CS. Formation and characteristics of Cu colloids from CuO powder by laser irradiation in 2-propanol. J Phys Chem B 1999;6851:57–103.
[30] Wu C, Mosher BP, Zeng T. One-step green route to narrowly dispersed copper nanocrystals. J Nanopart Res 2006;965:69–78.
[31] Slistan-Grijalvaa A, Herrera-Urbina R, Rivas-Silva JF, Valos-Borja MA, Castillon-Barraza FF, Posada-Amarillas A. Classical theoretical characterization of the surface plasmon absorption band for silver spherical nanoparticles suspended in water and ethylene glycol. Physica E 2005; 104:12–27.